



Polyrotaxane-based electrolyte with excellent thermal stability for quasi-solid lithium metal batteries

Jianmei Li¹ · Zijian Wang² · Qingsong Tong¹ · Luyi Yang² · Mengqi Zhu¹ · Hai Lin² · Feng Gao¹ · Jingzheng Weng¹

Received: 22 October 2021 / Revised: 5 May 2022 / Accepted: 12 May 2022 / Published online: 25 May 2022
© The Author(s), under exclusive licence to Springer-Verlag GmbH Germany, part of Springer Nature 2022

Abstract

Despite the high-energy densities, the safety problem of thermal runaway in lithium-ion batteries (LIBs) severely hinders their further application. Therefore, as an essential part of LIBs, the separator should ideally have good thermal stability at high temperatures. Here, a novel polyrotaxane (PR)-based gel polymer electrolyte (GPE) with good thermal stability is made by a simple solution casting method. The thermal shrinkage of the PR is less than 20% even heated at 200 °C; in contrast, the commercial Celgard 2400 separator undergoes dramatic deformation above 140 °C. The gel polymer electrolyte presents excellent compatibility in the cells of LiFePO₄ and LiNi_{0.5}Co_{0.2}Mn_{0.3}O₂ cathode. The cell composed of Li/GPE/LiFePO₄ presents good discharge performance and excellent stored performance. The cell composed of Li/GPE/LiNi_{0.5}Mn_{0.3}Co_{0.2}O₂ presents excellent capacity retention of 85.9% in 300 cycles while discharging at the 0.5 C rate. This GPE is promising to be applied to Li metal batteries with high safety and good cycle life.

Keywords Polyrotaxane · Gel polymer electrolyte · Thermal stability · Li anode · LiNi_{0.5}Mn_{0.3}Co_{0.2}O₂

Introduction

Lithium-ion batteries (LIBs) are one of the most promising energy storage systems due to their high energy density and long cycle life [1, 2]. However, potential safety hazards of LIBs due to thermal runaway of the separator and the leakage of the electrolyte remain a great challenge [3, 4]. Solid-state batteries have extensively been studied owing to their outstanding safety features [5]. However, the sluggish interfacial charge transfer has hindered their real application in market [6–8]. Thanks to the minimum leakage of electrolyte, gel polymer electrolytes (GPEs) with good interface contact, proper ionic conductivity, and good electrochemical window can reduce the embarrassment mentioned above [9–11].

In addition, GPE can inhibit the formation and growth of lithium dendrite to improve battery safety [12, 13]. GPE, including poly(vinylidene fluoride) (PVDF), poly(ethylene oxide) (PEO), poly(acrylonitrile) (PAN), and poly(methyl methacrylate) (PMMA), is a polymer electrolyte with liquid electrolyte as plasticizer dissolved in a polymer matrix [14, 15]. Among them, PVDF has been widely studied for its good film-forming properties and high electrochemical stability. However, its conductivity is low for the high crystallization (65 ~ 78%) in the PVDF-based GPE, limiting the application of PVDF in GPE. PEO is the earliest investigated polymer electrolytes due to its good mechanical properties and stability to lithium (Li) metal anode. Nevertheless, PEO has a high solubility in plasticizers and it could only couple with LiFePO₄ for its narrow electrochemical window [16], which limits its application [17]. Similar to the PVDF, PAN is also a polymer with good film-forming properties and can form a gel polymer electrolyte with a conductivity close to that of a liquid electrolyte. Unfortunately, C≡N in PAN has severe passivation on Li metal anode, which restrains its practical application [18]. Alternatively, PMMA has good stability for Li metal anode, but its mechanical properties are too poor to be applied [19].

To improve the safety risk of shrinkage of GPE at elevated temperature [20], many researchers have devoted to develop

Ms. Jianmei Li, Dr. Zijian Wang and Prof. Qingsong Tong contributed equally to the work.

✉ Qingsong Tong
qstong_3503@fjnu.edu.cn

¹ Fujian Provincial University Engineering Research Center of Efficient Battery Modules, College of Chemistry and Material Science, Fujian Normal University, Fuzhou 350007, People's Republic of China

² Shenzhen Graduate School, Peking University, Shenzhen 518055, People's Republic of China

the polymer matrix that is safe at high temperatures. Ali et al. developed a polymer matrix of PVDF-HFP/colloidal alumina via a phase inverse method, which is stable at 150 °C [21]. Liu et al. reported a thermal management polymer matrix by integrating BN with the 3D extrusion printing technique for Li metal batteries [22]. Recently, Ma et al. developed a coated AlPO_4 polypropylene (PP) with enhanced thermal stability for LIBs through a coating method [4]. Although above polymer matrixes exhibit high-temperature stability, GPEs have not widely applied in the commercial battery for their many disadvantages. They confront the weak mechanical strength and the safety risk of shrinkage at elevated temperature [23]. The plasticizers in GPEs are prone to volatilization and leakage at high temperature, which have a great impact on the life and stability of battery. Therefore, GPE that can balance shrinkage at elevated temperature, ionic conductivity, interface contact, electrochemical window, liquid electrolyte leakage, and compatibility is a better choice for lithium-ion batteries.

Another polymer type of polyrotaxane with the cyclodextrin (CD) molecule in the host–guest supramolecular [24, 25] was utilized as a binder in the silicon-carbon anode owing to the ability of slip and rotate around a polymer chain. Choi et al. found that the capacity fading rate of the silicon-carbon anode was suppressed while the cyclodextrin polyrotaxane was used as the binder. They considered that the polyrotaxane with a sliding-ring could alter the mechanical properties of the binder and lead to a highly elastic binder network engaging the sliding motion of polyrotaxane [26]. If the polyrotaxane is utilized as a polymer electrolyte, it might show exceptional electrochemical performance. Recently, Brunklaus et al. reported a grafted polyrotaxanes as solid polymer electrolytes (SPE) for lithium metal batteries (LMBs). However, the grafted polyrotaxane exhibits the low conductivity at room temperature. To raise the conductivity of grafted polyrotaxane to $1 \times 10^{-3} \text{ S cm}^{-1}$, it had to be heated to 60 °C. To consider that the particular structure of polyrotaxane, the novel polyrotaxanes (symbolized as PR) with the strong hydrogen bonds (O–H•••F) were firstly prepared from self-assembly of α -cyclodextrin (α -CD) host molecules threading onto polyethylene glycol (PEG) chains and blending with co-polymer poly(vinylidene-co-hexafluoropropylene) (P(VDF-HFP)). Then, the novel polyrotaxane-based electrolyte (symbolized as GPE) was further prepared from PR. Especially, the PR has excellent thermal stability to withstand the effect of the temperature as high as 200 °C. When coupled GPE with Li anode/ $\text{LiNi}_{0.5}\text{Mn}_{0.3}\text{Co}_{0.2}\text{O}_2$ (NMC532), excellent capacity retention of 85.9% was achieved after 300 cycles at 0.5 C rate. In addition, good dendrite suppression ability was presented by GPE in Li-symmetrical cells, demonstrating

the potential for high-energy-density Li metal batteries with high safety.

Experimental

Sample preparation

PR and GPE were prepared using below steps. Firstly, 1.0 g PEG ($M_w = 20,000$, Chemical Reagent Co. Ltd. of Chinese Medicine Group), 0.49 g α -CD ($M_w = 973$, Weifang Dakang Chem. Ind.), and 2.0 g PVDF-HFP ($M_w = 130,000$, Shenzhen Taotao Plasticizing Co., Ltd.) were separately dissolved into N,N-dimethyl formamide (DMF) at 80 °C. Then PEG solution, PVDF-HFP solution, and 0.21 g PEG ($M_w = 400$) were dropped into the α -CD solution slowly, followed by stirring for 24 h. After that, the solution was casted on a glass plate and dried on a vacuum oven at 60 °C to gain the dry polymer. Thirdly, the dry polymer was treated in deionized water for 20 min using an ultrasonic method and dry it to prepare the dry separator (PR) in the vacuum drier. Lastly, the GPE was obtained by soaking the PR in a plasticizer for 24 h and wiped out GPE with clean wiper. Unless stated otherwise, the plasticizer was composed of $1 \text{ mol L}^{-1} \text{ LiPF}_6$ and the mixture of ethylene carbonate (EC), ethyl methyl carbonate (EMC), and dimethyl carbonate (DEC) (1:1:1 by volume). To optimize the synthesis condition, the PR with other composition of different mass ratio (1:0.5, 1:1, 1:2, 1:3) of PEG and PVDF-HFP were prepared, and then further studied the composition effects on the electrochemical performance of the gel polymer electrolytes.

Characterization

The morphology of the PR separator was observed using a field emission scanning electron microscope (FESEM, TESCAN MIRA 3, Czech). X-ray patterns (XRD) of the sample were tested using an X-ray powder diffractometer (X'Pert PXR, PANalytical B.V.) at the voltage of 40 kV and current of 40 mA with a $K_{\alpha, \text{Cu}}$ radiation ($\lambda = 1.5406 \text{ \AA}$) in the 2θ range of 10–80°. Fourier transform infrared spectra (FTIR) of the sample were measured using a Thermo FTIR spectrometer (IS50, Nicolet) with a pressing potassium bromide troche. Proton nuclear magnetic resonance ($^1\text{H NMR}$) spectra of the sample were performed using a 400 MHz Bruker spectrometer using the $\text{DMSO-}d_6$ as solvent.

Differential scanning calorimetry (DSC) was measured using a differential thermal analyzer (DSC3, Mettler) at a heating rate of $10 \text{ }^\circ\text{C min}^{-1}$ from -50 to $150 \text{ }^\circ\text{C}$ in a N_2 atmosphere. Thermogravimetric analysis (TGA NETZSCHSTA449F3) was used to analyze the thermal stability of PR.

The absorbability of the PR separator was measured using following steps. The dry PR separator was soaked in the liquid electrolyte for 24 h after weighing, and excess electrolytes were wiped off. The absorbability (η) was calculated according to Eq. (1):

$$\eta = \frac{(W_2 - W_1)}{W_1} \times 100\% \tag{1}$$

where W_1 is the weight of pristine dry separator and W_2 is the weight of the separator after soaked in the liquid electrolyte.

The porosity of the PR separator was calculated according to Eq. (2):

$$\text{Porosity}(\%) = \frac{(W_t - W_o)}{\rho V} \times 100\% \tag{2}$$

where ρ is the density of n-butanol. V is the volume of the dry PR separator. The weight of the PR separator was measured before soaking (W_o) and after soaking (W_t) in a n-butanol for 2 h.

Thermal shrinkage of the PR separator was measured based on the dimensional change ratio while it was heated under various temperatures for 0.5 h, and was calculated according to Eq. (3) [4]:

$$\text{Thermalshrinkage}(\%) = \frac{(A - A_o)}{A_o} \times 100\% \tag{3}$$

where A_o and A refer to PR separator area before and after heated, respectively.

The tensile strength of the PR separator was measured by using a Digital-Display dynamometer (DS2-50 N, Japan).

Electrochemical measurements

Linear sweep voltammogram curves (LSV), electrochemical impedances (EIS), and cyclic voltammetry curves (CVs) of the GPE were tested by using the electrochemical work (CHI 604E, Shanghai Chenhua Instrument Co., Ltd.) in various cells (CR2025) [4] added 0.04 mL plasticizer during the assembling process of the cell. The LSV were tested with Li metal (Li)/GPE/stainless steel (SS) cell [4] at the scan rate of 1 mV s⁻¹.

The CVs were measured using the Li/GPE/LiFePO₄ composite cell [4] scanned at the scanning rate of 0.2 mV s⁻¹ and the LiFePO₄ composite was composed of LiFePO₄, conductive carbon (Super P), and polyvinylidene fluoride (PVDF) according to the weight ratio of 85:10:5. The content of the active material in the cathode was 1.5–1.7 mg cm⁻². LiFePO₄ bought from Energy Technology of Zhangzhou Wangbao Co. Ltd.

The EIS was measured in the frequency range from 1.0 × 10⁻² to 1.0 × 10⁵ Hz and the amplitude voltage was adjusted to 0.05 V. The Li⁺ diffusion coefficient of the GPE was tested with the Li/GPE/Li cell (CR2025). The Warburg coefficient of the impedance in low frequency region [4] (σ) was calculated according to Eq. (4), and the Li⁺ diffusion coefficient [4] (D_{Li^+}) was calculated according to Eq. (5).

$$-Z_{im} \propto \sigma \omega^{-\frac{1}{2}} \tag{4}$$

$$D_{Li^+} = \frac{(RT)^2}{2A^2 n^4 F^4 C^2 \sigma^2} \tag{5}$$

where σ is the Warburg coefficient of the impedance. R is gas constant (8.314 J mol⁻¹ K⁻¹). T is absolute temperature (298 K). A is the surface area ($S=1.766$ cm²). n is the number of electrons involved in electrode reaction ($n=1$). F is Faraday constant (96,485.3 C mol⁻¹). C is lithium-ion concentration ($C=1.0 \times 10^{-3}$ mol cm⁻³).

The ionic conductivity (σ) of GPE was tested with a SS/GPE/SS cell (CR2025) according to its electrochemical impedance spectroscopy (EIS), which can be calculated by using following Eq. (6) [4]:

$$\sigma = \frac{L}{R_b \times S} \tag{6}$$

Here, R_b is the bulk resistance; S and L are the area of the blocking stainless steel electrodes and the thickness of the GPE, respectively.

The lithium transference number (t_+) was determined by using a direct-current (DC) polarization and AC impedance measurements in a Li/GPE/Li symmetric cell. The t_+ was calculated using following equation:

$$t_+ = \frac{I_{ss} \times (\Delta V - I_o \times R_o)}{I_o \times (\Delta V \times I_o \times R_{ss})} \tag{7}$$

where I_o and I_{ss} are the initial and steady state currents; R_o and R_{ss} are the interface resistance in the initial and the steady state. ΔV is the applied voltage (10 mV).

The interface stability between lithium and electrolyte was evaluated in a symmetric Li/GPE/Li cell by lithium plating/stripping cycle experiment. Before the experiment, PR were immersed in plasticizer which was composed of 1 mol L⁻¹ LiPF₆ and the mixture of ethylene carbonate (EC), ethyl methyl carbonate (EMC), and dimethyl carbonate (DEC) (1:1:1 by volume). During the measurement process, the cell was activated with a current density of 0.1 mA cm⁻² in the first 20 h. Then it was measured with various currents.

The charge–discharge performances of button cell (CR2025) [4] were tested by using Neware battery testers (Neware BTS7.6.0). The button cell (CR2025) was composed of Li/GPE/cathode composite [4], in which the

cathode composite contained cathode material, conductive carbon (Super P), and polyvinylidene fluoride according to the weight ratio of 85:10:5. The button cells were assembled in an argon-filled glove box (Mikrouna, Universal) with the content of water and oxygen lower than 1 ppm.

Results and discussions

Physical characterization

The FTIR data of PEG, PVDF-HFP, α -CDs, and PR were shown in Fig. 1a and Table 1. Compared to the vibration of $-OH$ groups of the α -CDs (3400 cm^{-1}) and PEG (3440 cm^{-1}), that of the PR shifts to lower wavenumber (3029 cm^{-1} and 3022 cm^{-1}), indicating that the hydrogen bonds in the original α -CDs and PEG are broken, the new $O-H$ bonds and the stronger hydrogen bonds ($O-H\cdots F$) are formed in the PR. The ring vibration of α -CD in original α -CDs (952 cm^{-1}) slightly shifts to lower wavenumber (948 cm^{-1}), and symmetrical stretching vibration of $-CH_2$ in PEG (2890 cm^{-1}) shifts to lower wavenumber (2879 cm^{-1}) in PR, indicating that the molecular chain of the PEG inserts into the molecular ring of α -CDs. The vibration of $-CF_2-$ group in PVDF-HFP (1188 cm^{-1}) shifts to lower wavenumber (1180 cm^{-1}) in PR. The vibration of $-CF_3$ group in PVDF-HFP (1074 cm^{-1}) is almost same as that

in PR (1075 cm^{-1}), and that of HFP group in PVDF-HFP (881 cm^{-1}) is same as that in PR (881 cm^{-1}), indicating that the $-CF_2-$ group nor HFP group in PR forms the hydrogen bonds with the $-OH$ groups ($O-H\cdots F$) in α -CDs and PEG. Therefore, it can be confirmed that the polyrotaxane (PR) was successfully synthesized.

The surface morphology of the PR separator was observed by using a SEM technique (Fig. 1b), in which the pores on the surface of PR separator with the diameters from 0.2 to $2\text{ }\mu\text{m}$ can be observed for the dissolutions of PEG ($M_w=400$) in the dry polymer to deionized water. 1H NMR spectra (Fig. 1c) were used to investigate the formation mechanism of polyrotaxane, indicating that the 1H NMR of the CH in the α -CD is located at 4.8 ppm, and that of methylene groups in the PEG is at 3.5 ppm. Therefore, the PR had an inclusion ratio of ~ 32 CDs per PEG chain. XRD patterns of the PEG and α -CD show strong multi-peaks (Fig. 1d), indicating the PEG and α -CD possess high crystallization. Compared to the PEG and α -CD, XRD patterns of the PR separator exhibit weak single peak located around 20° of 2θ angles, which is in consistent with the result of the XRD patterns of the reaction product of α -CD and PEG ($M_w=1000$) without PVDF-HFP [31], indicating that the PEG crystal is disappeared [32] in PR separator for the crosslink reaction of PEG and α -CD. DSC curve (Fig. 1e) shows that the melting peak of the PEG crystals is disappeared in PR separator, which further verified that α -CD and PEG form PR crystal.

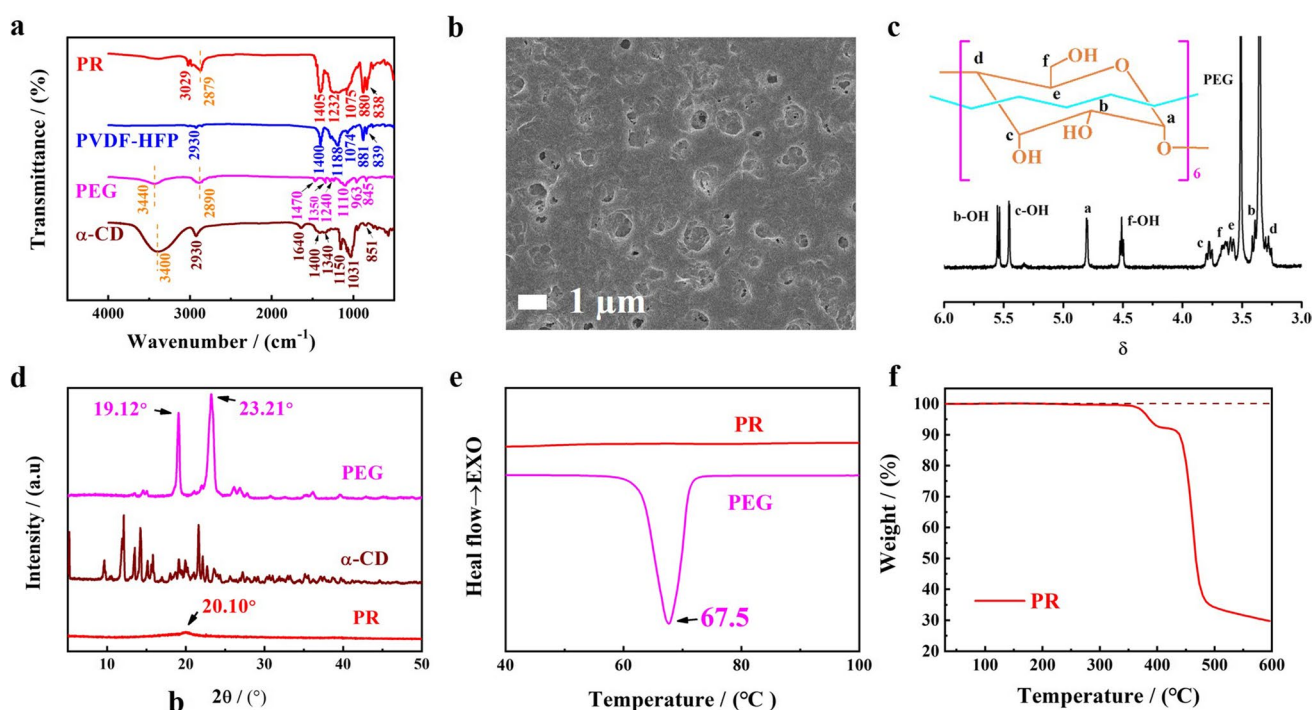


Fig. 1 a FTIR spectra of the samples; b SEM image of the PR separator; c 1H NMR spectra of PR; d XRD patterns of the samples; e DSC of the PEG and PR; f TAG curve of PR

Table 1 FTIR data of the samples

PR	α -CD	PEG	PVDF-HFP	Literature (cm ⁻¹)	Vibration mode and group
3029 (W), 3022 (M)		3440 (W)		3416 [28] 3396 [30]	Stretching vibration of –OH O–H
2980 (M)	3400 (S)		2930 (W)	2930 [29, 30]	CH ₂
2879 (M)	2930 (W)	2890 (M)		2882 [27]	Symmetrical stretching vibration of –CH ₂
	1640 (M)			1600~1680 [30]	Water in the cavity of CDs
1452 (W)		1470 (W)		1465 [28]	Bending vibration of –CH ₂ –
1405 (S)	1400 (M)		1400 (S)	1400 [29, 30]	–CH ₂ –
1331 (W)	1340 (W)	1350 (W)		1339 [28, 30]	Symmetrical deformation of –CH ₂
1232 (S)		1240 (W)		1278 [28], 1240 [28]	Bending vibration of O–H in PEG
1180 (S)			1188 (S)	1175 [29]	–CF ₂ –
	1150 (S)	1110 (M)		1080 [28, 30]	C–O
				1080~1120 [28]	Stretching of C–O of the secondary OH
				1100 [28, 30]	Stretching vibration of C–O
1075 (S)			1074 (W)	1073 [28]	–CF ₃
	1031 (M)			1036 [30]	Stretching of C–O
948 (W)	952 (W)	963 (W)		920~960 [30]	Ring vibration of α -CD
				946 [28]	In-plane deformation vibration of C–O
880 (S)			881 (S)	874 [29]	HFP
	851 (W)	845 (M)		840 [28, 30]	–CH ₂ –
838 (S)			839 (S)	838 [30]	C–F

W weak peak, M middle peak, S strong peak.

The thermal stability of PR was investigated by TAG. As shown in Fig. 1f, when the temperature exceeded 250 °C, PR has no significant weight loss rate. This indicated that PR had good thermal stability.

The images (Fig. 2a) show the shapes of the samples heated in the temperature range of 100 to 200 °C. As a comparison, the commercial separator (Celgard 2400) was treated under the same temperature range. It can be seen that both separators (PR and Celgard 2400) keep unchanging in size and shape while they were treated under the temperature below 140 °C. The thermal shrinkage of Celgard 2400 was rapidly increased while it was heated under the temperature higher than 150 °C and it was thoroughly melted while heated at 200 °C. The thermal shrinkages was 5.0% (Celgard 2400) and 3% (PR) while heated at 150 °C (Fig. 2b); it was 100% (Celgard 2400) and 20% (PR) while heated at 200 °C. Hu et al. [33] prepared a porous poly(ionic liquid)/PVDF-HFP composite separator via a simple and scalable phase inversion method, which shrinkage was 6.0% at 150 °C. Ahn et al. [34] prepared a reactive alumina-coated polyethylene (PE) and found that its thermal shrinkage was 3.0% at 140 °C. As we known, the lithium-ion battery shows the sandwich construction, if the shrinkage of the separator is higher than the limited value at the elevated temperature, the cathode and anode systems would be short-circuited, and even catch fire in battery systems. Therefore, the PR with excellent thermal stability, especially in the high temperature

zone, can effectively deal with thermal runaway of batteries. Figure 2c shows the measurement result of the tensile strength of the PR separator. The result shows that the tensile strength of the PR separator is 8.33 MPa. The further measurement shows that the PR exhibits the porosity of 31.5% and absorbability of 81.6%. Therefore, PR exhibits the high tensile strength, low porosity, and high absorbability. General knowledge shows that the mechanical strength of PR is decreased with the increasing of porosity for the decreasing of the thickness of hole wall. And the high porosity of PR is beneficial to the increasing of ionic conductivity of GPE. Many previous studies [35, 36] treaded to prepare high porosity polymer matrixes (i.e., PVDF, PEO etc.) to increase the ionic conductivity of gel polymer electrolytes. However, the gel polymer electrolytes with high porosity and low mechanical strength result in its high thermal shrinkage. Therefore, the gel polymer electrolytes that can balance high mechanical strength, high thermal stability, high ionic conductivity, low interface contact, and wide electrochemical window are the best choice for lithium-ion batteries. Compared to other gel polymer electrolytes, the polyrotaxane exhibits high tensile strength (PR) and ionic conductivity (GPE) under the condition of low porosity for strong hydrogen bonds (O–H•••F). Compared to the tensile strength of polypropylene separator (5.58 MPa) [4], the PR shows the obvious improved performance for its high tensile strength.

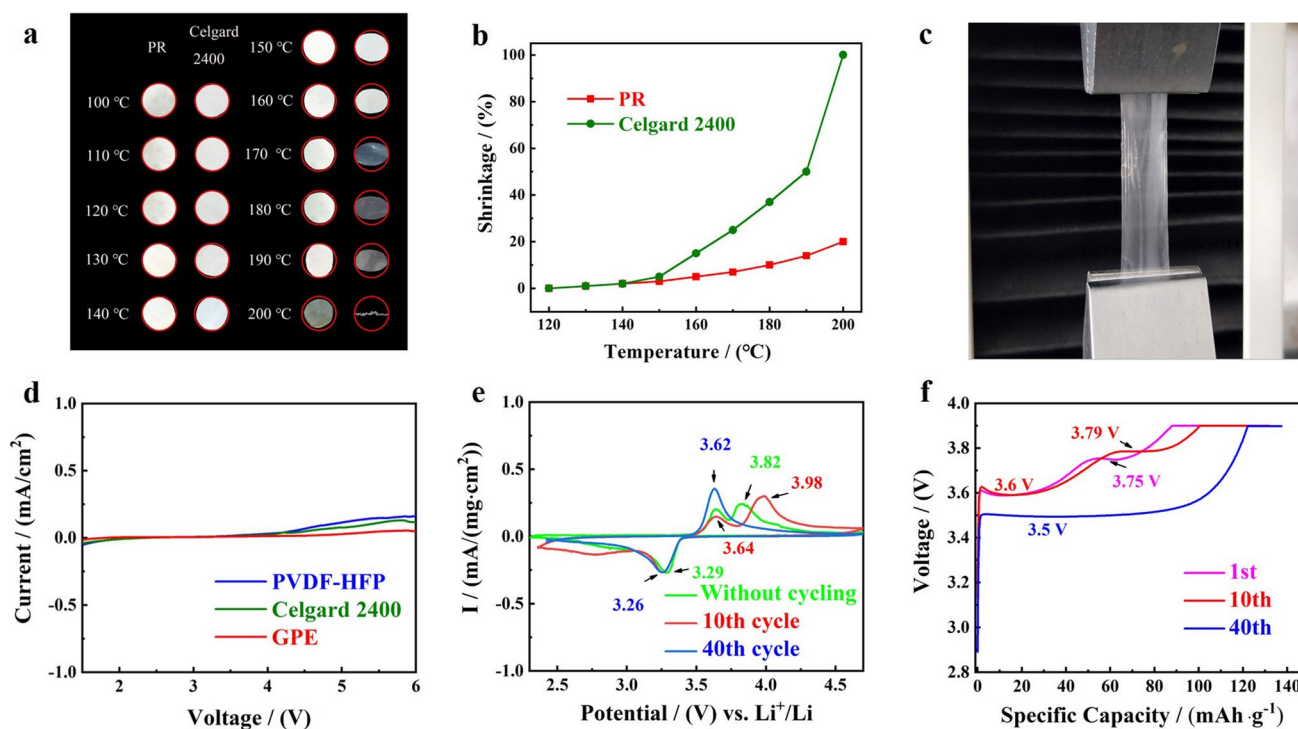


Fig. 2 Shape (a) and thermal shrinkage (b) of the sample heated in the temperature range of 100 to 200 °C; c measurement result of tensile strength of the PR; d LSV curves of the GPE, PVDF-HFP, Cel-

gard 2400; e CVs of the GPE cell after charge-discharge for various cycles; f charge profiles of LiFePO_4 cell at various cycles

Electrochemical performance

Figure 2d shows the LSV curve of the GPE, PVDF-HFP, and Celgard 2400. The oxidized potential of PVDF-HFP and Celgard 2400 is 4.2 V (vs. Li^+/Li). The one of PEO is 4.3 V (vs. Li^+/Li) [37]. Compared to PVDF-HFP, Celgard 2400, and PEO, the oxidized potential of GPE is higher than 5.25 V (vs. Li^+/Li) due to the cross-linking reaction between α -CD and PEG and strong hydrogen bonds ($\text{O}-\text{H}\cdots\text{F}$) in PR. Therefore, PR exhibits an obvious wider electrochemical stability window. Figure 2e shows the CVs of the GPE cells composed of $\text{Li}/\text{GPE}/\text{LiFePO}_4$ composites after charge-discharge for various cycles. Compared to normal LiFePO_4 system in the cell with liquid electrolyte [38], the redox reaction of LiFePO_4 cathode in GPE in the first 40 cycles presents difference reaction mechanism. In the cell without cycling and the one cycled for 10 cycles, the LiFePO_4 cathodes may be composed of complex I and complex II for the complex reaction between LiFePO_4 and hydrogen bonds group ($\text{O}-\text{H}\cdots\text{F}$) of GPE. It can be conjectured that the composition of complex I is $\text{LiFePO}_4-\text{F}\cdots\text{H}-\text{O}-\text{GPE}$, which corresponding to the oxidating potential of 3.64 V (vs. Li^+/Li) in CV curve; the composition of complex II is $\text{LiFePO}_4-\text{O}-\text{H}\cdots\text{F}-\text{GPE}$, which corresponding to the oxidating potential of higher 3.82 V (vs. Li^+/Li) in CV curve. During potential scanned from 2.5 to 4.6 V (vs. Li^+

Li), the oxidizing current of complex I is decreased with the increasing of the cycle number in the first 10 cycles, indicating that the oxidizing reaction of complex I ($\text{LiFePO}_4-\text{F}\cdots\text{H}-\text{O}-\text{GPE} \rightarrow \text{FePO}_4 + \text{Li}^+ + \text{F}\cdots\text{H}-\text{O}-\text{GPE}$) is gradually faded for the converting reaction from complex I to LiFePO_4 during the testing process of CV; the oxidizing current of complex I is increased with the increasing of the cycle number in the 11th cycle to 40th cycle, indicating that the oxidizing reaction of formed LiFePO_4 (at 3.62 V (vs. Li^+/Li)) in CV curve is activated. The oxidizing current of complex II ($\text{LiFePO}_4-\text{O}-\text{H}\cdots\text{F}-\text{GPE} \rightarrow \text{FePO}_4 + \text{Li}^+ + \text{O}-\text{H}\cdots\text{F}-\text{GPE}$) is increased with the increasing of cycle number in the first 10 cycles, indicating that the oxidizing reaction of complex II is gradually activated. However, the oxidating potential of complex II is moved from 3.82 V (vs. Li^+/Li) to 3.98 V (vs. Li^+/Li), indicating that the oxidating reaction is a non-reversible. The oxidizing current of complex II is faded with the increasing of cycle number in the 11th cycle to 40th cycle, verifying that the oxidating reaction is a non-reversible. The charged curves of LiFePO_4 cell exhibit two charged platforms, at around 3.6 V and 3.8 V (Fig. 2f), in the first 10 cycles. The charged curves of LiFePO_4 cell exhibit one charged platform (at around 3.55 V) in the 40th cycle. Therefore, above results of CV curve were verified by the result of the charge–discharge test. During the potential scanned from 4.6 V (vs. Li^+/Li) to 2.5 V (vs. Li^+/Li), the reducing reaction

at the potential around 3.29 V (vs. Li⁺/Li) corresponds the reaction (FePO₄ + Li⁺ → LiFePO₄) was almost unchanged in 40 cycles, indicating that the reducing reaction is reversible in 40 cycles.

EIS (Fig. 3a) are composed of two semicircles in high frequency region and a slope line with ~45° angle in low frequency region [4]. The cells (Li/GPE/LiFePO₄ composite) with various cycles have two small semicircles in the high frequency region, and the first semicircle may be caused by SEI film formed between GPE and lithium anode. According to the EIS data (Fig. 3a) and its equivalent circuit (Fig. 3c), the charge-transfer resistance inside cells was calculated as 205 Ω (without cycling), 140 Ω (after 10 cycles), and 76 Ω (after 40 cycles), respectively. The charge-transfer resistance inside cells [39, 40] was decreased with the increasing of cycle number, indicating that the compatibility is improved between LiFePO₄ composite and GPE. The Warburg coefficient (σ) of the impedance (Li/GPE/Li cell) in low frequency region (Fig. 3b) [4] can be calculated according to Eq. (4). Then the Li⁺ diffusion coefficient of the GPE (D_{Li^+}) calculated was $4.36 \times 10^{-12} \text{ cm}^2 \text{ s}^{-1}$ according to Eq. (5). The Li⁺ diffusion coefficient of the gel polymer electrolyte [41] was $2.2 \times 10^{-12} \text{ cm}^2 \text{ s}^{-1}$, which composed of bifunctional ionic liquid, poly(diallyldimethylammonium) bis(trifluoromethanesulfonyl)imide, high lithium-concentration phosphonium ionic liquid, and trimethyl(isobutyl) phosphonium bis(fluorosulfonyl)-imide. The coated

polypropylene separator [4] exhibits the Li⁺ diffusion coefficient of $4.64 \times 10^{-13} \text{ cm}^2 \text{ s}^{-1}$. That indicates the cell using GPE may present excellent Li⁺ diffusion performance during charge-discharging procedure.

According to Fig. 3d (SS/GPE/SS cell) and Eq. (6), the study results show that the mass ratio of PEG and PVDF-HFP has the obvious effect on the ionic conductivity. The ionic conductivity of GPE is $6.65 \times 10^{-5} \text{ S cm}^{-1}$ ($W_{\text{PEG}}:W_{\text{PVDF-HFP}} = 1:0.5$), $7.00 \times 10^{-5} \text{ S cm}^{-1}$ ($W_{\text{PEG}}:W_{\text{PVDF-HFP}} = 1:1$), and $1.73 \times 10^{-4} \text{ S cm}^{-1}$ ($W_{\text{PEG}}:W_{\text{PVDF-HFP}} = 1:2$), respectively. While the mass ratio of PEG and PVDF-HFP is higher than 1:2, the as-prepared GPE shows non-homogeneous composition for the low solubility of PVDF-HFP in the solution. Therefore, the GPE ($W_{\text{PEG}}:W_{\text{PVDF-HFP}} = 1:2$) is the optimization mass ratio. The conductivity reported here is obviously higher than that of previous polymer electrolytes at room temperature (e.g., $6.89 \times 10^{-5} \text{ S cm}^{-1}$ [42] and $2.23 \times 10^{-5} \text{ S cm}^{-1}$ at 25 °C [43], $1 \times 10^{-3} \text{ S cm}^{-1}$ at 60 °C (grafted polyrotaxane)) [27]. To explore the electrochemical performance of GPE at different temperature, the ionic conductivities at different temperature were shown in Fig. 3e, indicating that the ionic conductivities of GPE are $1.92 \times 10^{-4} \text{ S cm}^{-1}$ (20 °C), $2.51 \times 10^{-4} \text{ S cm}^{-1}$ (40 °C), $4.28 \times 10^{-4} \text{ S cm}^{-1}$ (60 °C), and $5.82 \times 10^{-4} \text{ S cm}^{-1}$ (80 °C), respectively. With the increase of temperature in the temperature range of 20 to 80 °C, the ionic conductivity is gradually improved, which verifies that

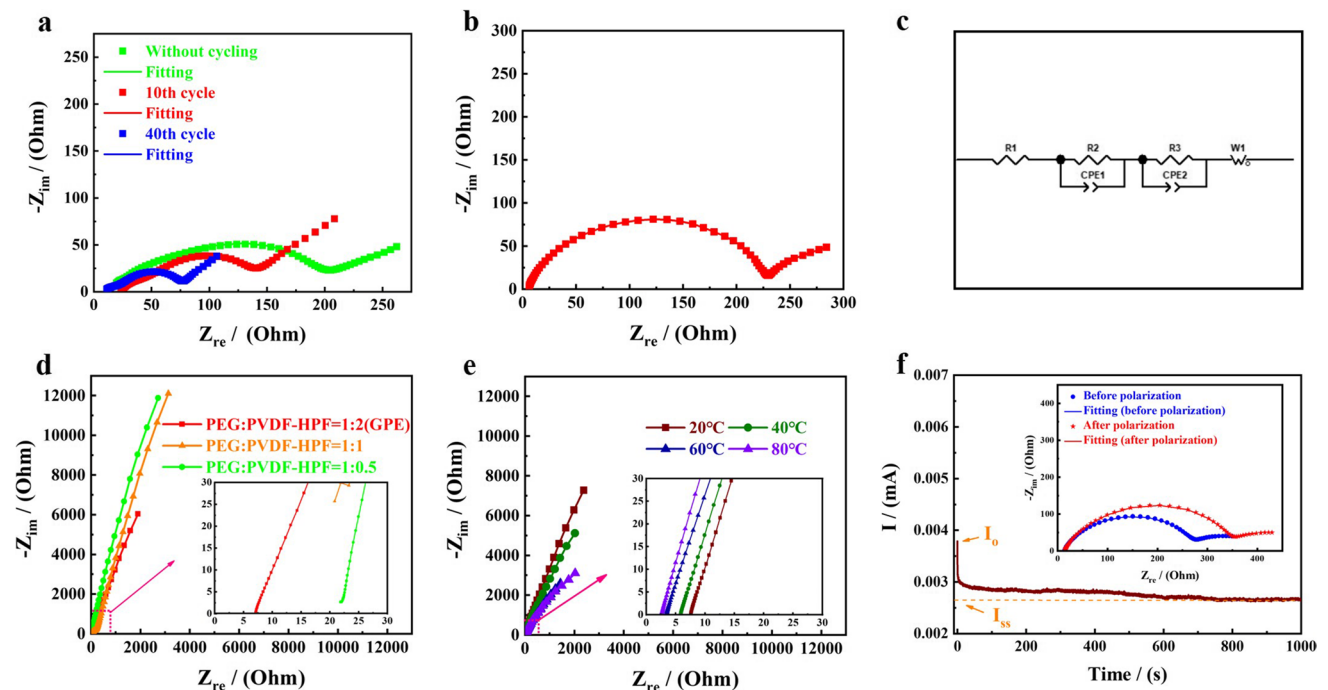


Fig. 3 EIS (a) and the equivalent circuit (c) of the Li/GPE/LiFePO₄ composite cells after various cycles; **b** EIS of the Li/GPE/Li cell; **d** EIS of the SS/GPE/SS cell; **e** EIS of SS/GPE/SS cell at different tem-

perature; **f** current–time curve and impedance spectra (insert image) before and after polarization of a symmetric cell of Li/GPE/Li

the heating can improve the transport of lithium ions [27, 44]. The Li^+ transference number (t_+) is calculated as 0.69 at 25 °C according to the results of the chronoamperometric measurement and AC impedance (Fig. 3f) and Eq. (7), which is superior to other gel polymer electrolytes (e.g., PVDF-HFP-based gel polymer electrolyte: 0.57 [45] and poly(ethylene oxide)-based composite gel polymer electrolytes: 0.55 [46]).

Figure 4a and b show the voltage–time profiles of the Li/GPE/Li cells at a current density of 0.5 mA cm^{-2} with a capacity of 0.5 mAh cm^{-2} or 1 mA cm^{-2} with a capacity of 1 mAh cm^{-2} , respectively, after these cells were handled with the current of 0.1 mA cm^{-2} with a capacity of 0.1 mAh cm^{-2} for 20 h. The performance of resistance to Li dendrite puncture could be analyzed by the Li/GPE/Li cells, in which the plasticizer is $1 \text{ mol L}^{-1} \text{ LiPF}_6$ in a mixture of ethylene carbonate (EC) and dimethyl carbonate (DEC) (1:1 by volume). The activation phenomenon [47] can be noticed from the voltage profile of 0.5 mA cm^{-2} with a capacity of 0.5 mAh cm^{-2} , where the voltage slowly reduces from about 160 to 50 mV in the first 50 h and then becomes stable (Fig. 4a). The cell with GPE presents stable voltage polarization of 34 mV over 400 h of cycling without short-circuiting. When the applied current increased to 1 mA cm^{-2} with a capacity of 1 mAh cm^{-2} , the voltage polarization was increased to 58 mV and over 200 h of cycling (Fig. 4b), indicating a good dendrite suppression performance. To explore the good

lithium dendrite inhibition performance of GPE, SEM tests were conducted with the surface of lithium anode. From Fig. 4c and d, the surfaces of lithium anodes were smooth without any dendrites on the surface of lithium anode without cycling (Fig. 4c) and after cycling 80 h in Li/GPE/Li symmetric cell. Those proved that GPE possessed good interfacial stability with Li metal anodes and can effectively restrain Li dendrites.

Charge–discharge performance

Charge–discharge performance in the cell with LiFePO_4

Figure 5a shows cycling performances of the fresh cell at the 1 C rate at various temperatures, indicating that the cell using LiFePO_4 cathode and GPE presented the first cycle capacities of 127 mAh g^{-1} (25 °C), 150 mAh g^{-1} (55 °C), and 151 mAh g^{-1} (80 °C), respectively. The initial coulomb efficiency was 84% (25 °C), 73% (55 °C), and 64% (80 °C), respectively. The low coulombic efficiency of the cell at 80 °C may be related to the side reaction, such as the side reaction of complex I and complex II between LiFePO_4 and GPE. During the charge–discharge cycling, the fresh cell (80 °C) increased the discharged capacity, then decreased the discharged capacity with the increasing of cycle number, indicating that the charge–discharge process has an active procedure. After 40 cycles, the fresh cell does not have any

Fig. 4 Voltage–time profiles of the cells of Li/GPE/Li at a current of 0.5 mA cm^{-2} with a capacity of 0.5 mAh cm^{-2} (a) and 1 mA cm^{-2} (b) with a capacity of 1 mAh cm^{-2} , respectively; SEM images of lithium metal surface without cycling (c) and after cycling 80 h of Li/GPE/Li symmetric cell (d)

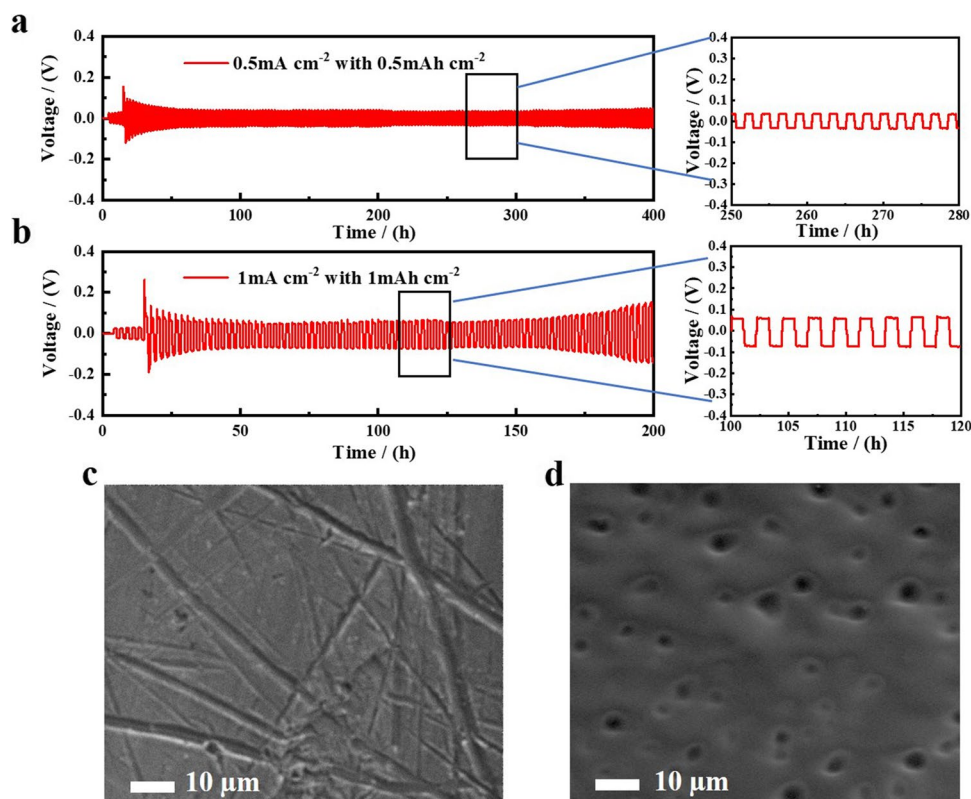
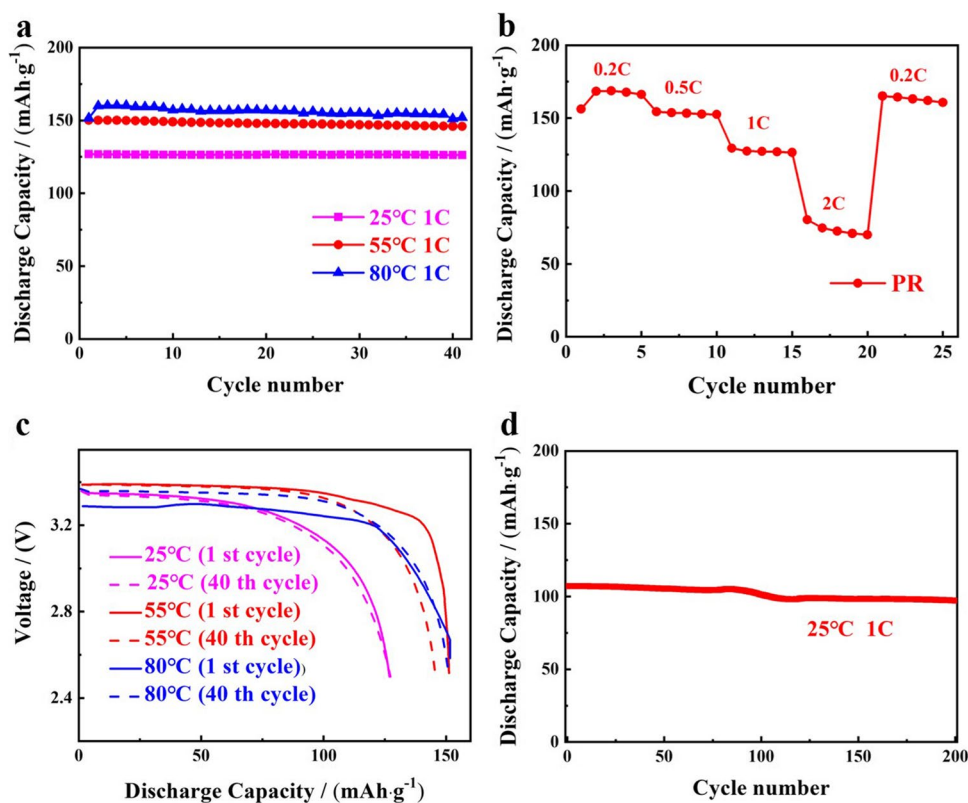


Fig. 5 **a** Cycling performance of the fresh cell at the 1 C rate and various temperatures; **b** cycling performance of the fresh cell charge-discharged continuously for 24 cycles at various rates; **c** voltage profiles of the fresh cells at various temperatures and rates; **d** long-term cycle performance of the stored cell (after 40 cycles at 55 °C at the 1 C rate and stored for 1 month) at 25 °C



capacity fading at 25 °C; it presents the capacity retention rate of 97.4% at 55 °C and 94.2% at 80 °C, respectively. The result shows that the GPE has good compatibility under high temperature. Figure 5c shows the voltage profiles of the fresh cell at the 1 C rate and various temperatures, indicating that the discharge voltage platform of the fresh cell was located at 3.38 V (25 °C), 3.39 V (55 °C), and 3.29 V (80 °C) in the 1st cycle, and at 3.34 V (25 °C), 3.39 V (55 °C), and 3.36 V (80 °C) at the 40th cycle. The cell presents high discharge voltage platform, indicating that the GPE electrolyte presents low polarization during discharging procedure.

Figure 5b shows the rate performance of the fresh cell at current densities of 0.2 C, 0.5 C, 1 C, and 2 C, respectively. Its discharge capacities are 168 mAh g⁻¹ (0.2 C), 153 mAh g⁻¹ (0.5 C), 127 mAh g⁻¹ (1 C), and 72 mAh g⁻¹ (2 C), respectively. The results show that the fresh cell presents good rate performance. Xie et al. [48] tested the charge–discharge performance of the Li/solid polymer electrolytes/LiFePO₄ cell, which the solid polymer electrolytes were composed of PEO, LiTFSI, and TBPHP (tetrabutylphosphonium 2-hydroxypyridine). Their results showed the discharge capacities of 129.7 mA h g⁻¹ (0.2 C), 113.7 mA h g⁻¹ (0.5 C), 80.7 mA h g⁻¹ (1 C), and 64.9 mA h g⁻¹ (2 C), respectively, at 50 °C. Compared to the result of Xie et al. [48], the GPE presents obviously higher rate performance. As shown in Fig. 5d, the long-term cycle performance of the stored cell at the 1 C rate was tested at 25 °C, in which the stored cell

was obtained by charge-discharged it for 40 cycles at 55 °C at the 1 C rate and stored for 1 month in advance. The stored cell presents the discharge capacities of 107 mAh g⁻¹ (1st cycle) and 97 mAh g⁻¹ (200th cycle); the capacity fading rate is 9.3% in 200 cycles. Compared to the data in Fig. 5a, the stored cell presents excellent cycling stability though the stored cell has lower discharge capacity at 25 °C. The stored cell has good cyclic stability, indicating that the interface reaction between GPE and LiFePO₄ cathode is not obvious, and the self-discharge rate is low. It can be conjectured that the strong hydrogen bonds (O–H...F) formed in the GPE obviously decrease the reaction activity between GPE and LiFePO₄ cathode during storage process. Till now, less study pays close attention to the storage performance of the polymer electrolyte due to the obvious increasing of the surface impedance with the increasing of storage time. Therefore, the cell using LiFePO₄ cathode and GPE presents excellent cycling stability and stored performance, indicating that the GPE presents excellent stability in the cell of LiFePO₄.

Charge–discharge performance in the cell with LiNi_{0.5}Co_{0.2}Mn_{0.3}O₂ (NMC532)

The charge–discharge performance of GPE was also evaluated by the cell composed of Li/GPE/NMC532 (LiNi_{0.5}Co_{0.2}Mn_{0.3}O₂) cathode with the plasticizer composed of 1 mol L⁻¹ LiPF₆ in a mixture of ethylene carbonate (EC)

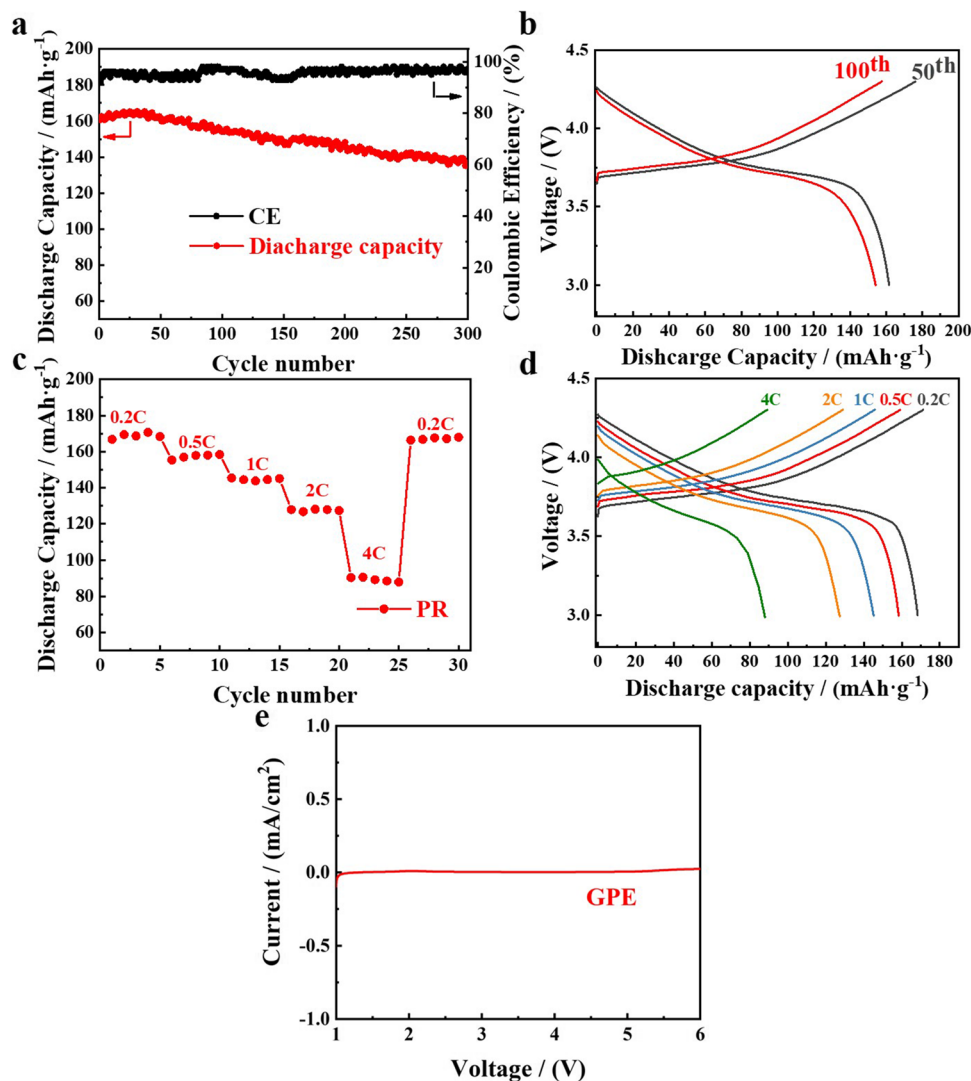
and dimethyl carbonate (DEC) (1:1 by volume). As shown in Fig. 6a, the Li/NMC532 cell with the GPE presents high-capacity retention of 85.9% after 300 cycles at the 0.5 C rate with relatively stable coulombic efficiency (CE). The voltage profiles of the 50th cycle and 100th cycle (Fig. 6b) present its weak voltage hysteresis and less increase with the cycling. Figure 6c shows the rate capability of the Li/NMC532 cells with the GPE. The obtained discharge capacity was 168.3 mAh g^{-1} (0.2 C rate), 158.4 mAh g^{-1} (0.5 C), 145.1 mAh g^{-1} (1 C), 127.3 mAh g^{-1} (2 C), and 88 mAh g^{-1} (4 C), respectively. As the discharge current was recovered to 0.2 C, the discharge capacity was still as high as 168 mAh g^{-1} , presenting good cycling stability and reversibility. Charge/discharge voltage profiles of the Li/GPE/NMC532 composite cell were also showed in Fig. 6d. The discharge voltage platforms are 3.74 V (0.2 C), 3.73 V (0.5 C), 3.73 V (1 C), 3.73 V (2 C), and 3.67 V (4 C), respectively, indicating that the Li/GPE/NMC532 composite cell presents the excellent high-rate performance. Previous study exhibits that

the oxidized potential of PEO is 4.05 V [49]. LSV curves of the GPE showed in Fig. 6e; the oxidized potential of GPE is higher than 5.25 V, indicating that the GPE exhibits excellent antioxidation.

Conclusions

In summary, a polyrotaxane-based gel polymer electrolyte (GPE) with the micro hole was firstly prepared by using PEG, α -CD, and PVDF-HFP with a quite simple solution casting method. In the Li/GPE/LiFePO₄ composite cell, the sample presents a capacity of 127 mAh g^{-1} in the first cycle and no obvious capacity fading was observed after 40 cycles at the 1 C rate. The stored cell obtained after 40 cycles at 55 °C and stored for 1 month at 25 °C presents discharge capacities of 107 mAh g^{-1} (1st cycle) and 97 mAh g^{-1} (200th cycle). The capacity fading rate of the stored cell is only 0.047% per cycle in 200 cycles. When

Fig. 6 **a** Cycling performance of Li/GPE/NMC532 cells; **b** voltage profiles of the Li/GPE/NMC532 cells; **c** rate capability of the Li/GPE/NMC532 cells; **d** discharge/charge curves of the Li/GPE/NMC532 cells at various rates; **e** LSV curves of the GPE



the prepared GPE was coupled with high-voltage cathode $\text{LiNi}_{0.5}\text{Co}_{0.2}\text{Mn}_{0.3}\text{O}_2$, excellent capacity retention of 85.9% was obtained after 300 cycles at the 0.5 C rate as well as a good rate capability. The GPE showed strong resistance to Li dendrite puncture. The GPE presents tensile strength of 8.33 MPa, thermal shrinkage of 20% at 200 °C, and excellent compatibility in the LiFePO_4 and $\text{LiNi}_{0.5}\text{Co}_{0.2}\text{Mn}_{0.3}\text{O}_2$ system due to the strong hydrogen bonds between $-\text{CF}_2$ in PR and $-\text{OH}$ of α -CDs and PEG (inclusion ratio: ~ 32 CDs per PEG chain). Therefore, the GPE with excellent thermal stability in this work is expected to be an ideal gel polymer electrolyte to achieve high-voltage and middle-voltage Li metal batteries.

Funding This work was supported by the Fujian Provincial Science and Technology Department's University Industry Cooperation Project (grant nos. 2016H6006, 2020H6010) and Fuzhou Science and Technology Bureau Project (grant no. 2017-G-68).

References

- Lu J, Chen Z, Pan F, Cui Y, Amine K (2018) High-performance anode materials for rechargeable lithium-ion batteries. *Electrochem Energy Rev* 1:35–53. <https://doi.org/10.1007/s41918-018-0001-4>
- Xiang J, Yang L, Yuan L, Yuan K, Zhang Y, Huang Y, Lin J, Pan F, Huang Y (2019) Alkali-metal anodes: from lab to market. *Joule* 3:2334–2363. <https://doi.org/10.1016/j.joule.2019.07.027>
- Tarascon JM, Armand M (2001) Issues and challenges facing rechargeable lithium batteries. *Nature* 414:359–367. <https://doi.org/10.1038/35104644>
- Ma S, Lin H, Yang L, Tong Q, Pan F, Weng J, Zheng S (2019) High thermal stability and low impedance polypropylene separator coated with aluminum phosphate. *Electrochim Acta* 320:134528. <https://doi.org/10.1016/j.electacta.2019.07.039>
- Song Y, Yang L, Zhao W, Wang Z, Zhao Y, Wang Z, Zhao Q, Liu H, Pan F (2019) Solid-state electrolytes: revealing the short-circuiting mechanism of garnet-based solid-state electrolyte. *Adv Energy Mater* 9:1970076. <https://doi.org/10.1002/aenm.20190671>
- Wang K, Yang L, Wang Z, Zhao Y, Wang Z, Han L, Song Y, Pan F (2018) Enhanced lithium dendrite suppressing capability enabled by a solid-like electrolyte with different-sized nanoparticles. *Chem Commun* 54:13060–13063. <https://doi.org/10.1039/c8cc07476c>
- Wang Z, Wang Z, Yang WH, Song Y, Han L, Yang K, Hu J, Chen H, Pan F (2018) Boosting interfacial Li^+ transport with a MOF-based ionic conductor for solid-state batteries. *Nano Energy* 49:580–587. <https://doi.org/10.1016/j.nanoen.2018.04.076>
- Yang L, Wang Z, Feng Y, Tan R, Zuo Y, Gao R, Zhao Y, Han L, Wang Z, Pan F (2017) Flexible composite solid electrolyte facilitating highly stable “soft contacting” Li-electrolyte interface for solid state lithium-ion batteries. *Adv Energy Mater* 7:1701437. <https://doi.org/10.1002/aenm.201701437>
- Jaumaux P, Liu Q, Zhou D, Xu X, Wang G (2020) Deep eutectic solvent-based self-healing polymer electrolyte for safe and long-life lithium metal batteries. *Angew Chem Int Ed* 59:9134–9142. <https://doi.org/10.1002/anie.202001793>
- Gong S, Huang Y, Cao H, Lin Y, Li Y, Tang S, Wang M, Li X (2016) A green and environment-friendly gel polymer electrolyte with higher performances based on the natural matrix of lignin. *J Power Sources* 307:624–633. <https://doi.org/10.1016/j.jpowsour.2016.01.030>
- Wu J, Wang X, Liu Q, Wang S, Zhou D, Kang F (2021) A synergistic exploitation to produce high-voltage quasi-solid-state lithium metal batteries. *Nat Commun* 12:5746. <https://doi.org/10.1038/s41467-021-26073-6>
- Ren W, Ding C, Fu X, Huang Y (2021) Advanced gel polymer electrolytes for safe and durable lithium metal batteries: challenges, strategies, and perspectives. *Energy Stor Mater* 34:515–535. <https://doi.org/10.1016/j.ensm.2020.10.018>
- Zhou D, Shanmukaraj D, Tkacheva A, Armand M, Wang G (2019) Polymer electrolytes for lithium-based batteries: advances and prospects. *Chem* 5:2326–2352. <https://doi.org/10.1016/j.chempr.2019.05.009>
- Zhu M, Wu J, Wang Y, Song M, Long L, Siyal SH, Yang X, Sui G (2019) Recent advances in gel polymer electrolyte for high-performance lithium batteries. *J Energy Chem* 37:126–142. <https://doi.org/10.1016/j.jechem.2018.12.013>
- Song JY, Wang YY, Wan CC (1999) Review of gel-type polymer electrolytes for lithium-ion batteries. *J Power Sources* 77:183–197. [https://doi.org/10.1016/s0378-7753\(98\)00193-1](https://doi.org/10.1016/s0378-7753(98)00193-1)
- Zhu L, Li J, Jia Y, Zhu P, Jing M, Yao S, Shen X, Li S, Tu F (2020) Toward high performance solid-state lithium-ion battery with a promising PEO/PPC blend solid polymer electrolyte. *Int J Energy Res* 44(13):10168–10178. <https://doi.org/10.1002/er.5632>
- Xue Z, Xie D, He X (2015) Poly(ethylene oxide)-based electrolytes for lithium-ion batteries. *J Mater Chem A3*:19218–19253. <https://doi.org/10.1039/c5ta03471j>
- Hu P, Chai J, Duan Y, Liu Z, Cui G, Chen L (2016) Progress in nitrile-based polymer electrolytes for high performance lithium batteries. *J Mater Chem A4*:10070–10083. <https://doi.org/10.1039/c6ta02907h>
- Zhang H, Zhang J, Ma J, Xu G, Dong T, Cui G (2019) Polymer electrolytes for high energy density ternary cathode material-based lithium batteries. *Electrochem Energy Rev* 2:128–148. <https://doi.org/10.1007/s41918-018-00027-x>
- Waqas M, Ali S, Feng C, Chen D, Han J, He W (2019) Recent development in separators for high-temperature lithium-ion batteries. *Small* 15:1901689. <https://doi.org/10.1002/sml.201901689>
- Ali S, Tan C, Waqas M, Lv W, Wei Z, Wu S, Boateng B, Liu J, Ahmed J, Xiong J, Goodenough JB, He W (2018) Highly efficient PVDF-HFP/colloidal alumina composite separator for high-temperature lithium-ion batteries. *Adv Mater Inter* 5:1701147. <https://doi.org/10.1002/admi.201701147>
- Liu Y, Qiao Y, Zhang Y, Yang Z, Gao T, Kirsch D, Liu B, Song J, Yang B, Hu L (2018) 3D printed separator for the thermal management of high-performance Li metal anodes. *Energy Stor Mater* 12:197–203. <https://doi.org/10.1016/j.ensm.2017.12.019>
- Long L, Wang S, Xiao M, Meng Y (2016) Polymer electrolytes for lithium polymer batteries. *J Mater Chem A* 4:10038–10069. <https://doi.org/10.1039/c6ta02621d>
- Harada A, Okada M, Kawaguchi Y, Kamachi M (1999) Macromolecular recognition: new cyclodextrin polyrotaxanes and molecular tubes. *Polym Adv Technol* 10:3–12. [https://doi.org/10.1002/\(sici\)1099-1581\(199901/02\)10:1/2%3c3::aid-pat759%3e3.0.co;2-s](https://doi.org/10.1002/(sici)1099-1581(199901/02)10:1/2%3c3::aid-pat759%3e3.0.co;2-s)
- Harada A, Li J, Kamachi M, Kitagawa Y, Katsube Y (1997) Structures of polyrotaxane models. *Carbohydr Res* 305:127–129. [https://doi.org/10.1016/s0008-6215\(97\)00276-0](https://doi.org/10.1016/s0008-6215(97)00276-0)
- Choi S, Kwon TW, Coskun A, Choi JW (2017) Highly elastic binders integrating polyrotaxanes for silicon microparticle anodes in lithium-ion batteries. *Science* 357:279–283. <https://doi.org/10.1126/science.aal4373>

27. Imholt L, Dörr TS, Zhang P, Ibing L, Cekic-Laskovic I, Winter M, Brunklaus G (2019) Grafted polyrotaxanes as highly conductive electrolytes for lithium metal batteries. *J Power Sources* 409:148–158. <https://doi.org/10.1016/j.jpowsour.2018.08.077>
28. Chen G, Xu Y, Shi T, Wu X (2019) Preparation and properties of polyacrylonitrile/polyethylene glycol composite fibers phase change materials by centrifugal spinning. *Mater Res Express* 6:095502. <https://doi.org/10.1088/2053-1591/ab2d0a>
29. Dognani G, Hadi P, Ma H, Cabrera FC, Job AE, Agostini DLS, Hsiao BS (2019) Effective chromium removal from water by polyaniline-coated electrospun adsorbent membrane. *Chem Eng J* 372:341–351. <https://doi.org/10.1016/j.cej.2019.04.154>
30. Senra JD, Malta LFB, Costa MEHM, Michel RC, Aguiar LCS, Simas ABC, Antunes OAC (2009) Hydroxypropyl- α -cyclodextrin-capped palladium nanoparticles: active scaffolds for efficient carbon-carbon bond forming cross-couplings in water. *Adv Synth Catal* 351(14–15):2411–2422. <https://doi.org/10.1002/adsc.200900348>
31. Harada A, Kamachi M (1990) Complex formation between poly(ethylene glycol) and α -cyclodextrin. *Macromolecules* 23(10):2821–2823. <https://doi.org/10.1021/ma00212a039>
32. Lin Y, Ito K, Yokoyama H (2018) Solid polymer electrolyte based on crosslinked polyrotaxane. *Polymer* 136:121–127. <https://doi.org/10.1016/j.polymer.2017.12.046>
33. Hu Z, Chen J, Guo Y, Zhu J, Qu X, Niu W, Liu X (2020) Fire-resistant, high-performance gel polymer electrolytes derived from poly(ionic liquid)/P(VDF-HFP) composite membranes for lithium ion batteries. *J Membr Sci* 599:117827. <https://doi.org/10.1016/j.memsci.2020.117827>
34. Ahn JH, You T, Lee S, Esken D, Dehe D, Huang Y, Kim D (2020) Hybrid separator containing reactive, nanostructured alumina promoting in-situ gel electrolyte formation for lithium-ion batteries with good cycling stability and enhanced safety. *J Power Sources* 472:228519. <https://doi.org/10.1016/j.jpowsour.2020.228519>
35. Zhang Q, Liu Y, Ma J, Zhang M, Ma X, Chen F (2019) Preparation and characterization of polypropylene supported electrospun POSS-(C3H6Cl)8/PVDF gel polymer electrolytes for lithium-ion batteries. *Colloids Surf A* 580:123750. <https://doi.org/10.1016/j.colsurfa.2019.123750>
36. Forbey SJ, Divoux GM, Moore KE, Moore RB (2015) Cross-linked electrospun poly(ethylene oxide) fiber mats as structured polymer-gel electrolyte. *ECS Trans* 66(35):1–15. <https://doi.org/10.1149/06635.0001ecst>
37. Fan Z, Ding B, Zhang T, Lin Q, Malgras V, Wang J, Dou H, Zhang X, Yamauchi Y (2019) Solid/solid interfacial architecturing of solid polymer electrolyte-based all-solid-state lithium-sulfur batteries by atomic layer deposition. *Small* 15(46):1903952. <https://doi.org/10.1002/smll.201903952>
38. Yu J, He Y, Zou S, Na B, Liu H, Liu J, Li H (2020) Redox-active manganese dioxide@polypropylene hybrid separators for advanced lithium ion batteries. *Appl Surf Sci* 508:144757. <https://doi.org/10.1016/j.apsusc.2019.144757>
39. Liu B, Huang Y, Cao H, Zhao L, Huang Y, Song A, Lin Y, Li X, Wang M (2018) A novel porous gel polymer electrolyte based on poly(acrylonitrile-polyhedral oligomeric silsesquioxane) with high performances for lithium-ion batteries. *J Membr Sci* 545:140–149. <https://doi.org/10.1016/j.memsci.2017.09.077>
40. Liu B, Huang Y, Zhao L, Huang Y, Song A, Lin Y, Wang M, Li X, Cao H (2018) A novel non-woven fabric supported gel polymer electrolyte based on poly(methylmethacrylate-polyhedral oligomeric silsesquioxane) by phase inversion method for lithium ion batteries. *J Membr Sci* 564:62–72. <https://doi.org/10.1016/j.memsci.2018.07.014>
41. Guan X, Wu Q, Zhang X, Guo X, Li C, Xu J (2020) In-situ crosslinked single ion gel polymer electrolyte with superior performances for lithium metal batteries. *Chem Eng J* 382:122935. <https://doi.org/10.1016/j.cej.2019.122935>
42. Fu X, Shang C, Yang M, Akinoglu EM, Wang X, Zhou G (2020) An ion-conductive separator for high safety Li metal batteries. *J Power Sources* 475:228687. <https://doi.org/10.1016/j.jpowsour.2020.228687>
43. Chai J, Liu Z, Ma J, Wang J, Liu X, Liu H, Zhang J, Cui G, Chen L (2017) In situ generation of poly(vinylene carbonate) based solid electrolyte with interfacial stability for LiCoO₂ lithium batteries. *Adv Sci* 4(2):1600377. <https://doi.org/10.1002/advs.201600377>
44. Song A, Huang Y, Zhong X, Cao H, Liu B, Lin Y, Wang M, Li X (2017) Gel polymer electrolyte with high performances based on pure natural polymer matrix of potato starch composite lignocellulose. *Electrochim Acta* 245:981–992. <https://doi.org/10.1016/j.electacta.2017.05.176>
45. Jie J, Liu Y, Cong L, Zhang B, Lu W, Zhang X, Liu J, Xie H, Sun L (2020) High-performance PVDF-HFP based gel polymer electrolyte with a safe solvent in Li metal polymer battery. *J Energy Chem* 49:80–88. <https://doi.org/10.1016/j.jechem.2020.01.019>
46. Gao H, Huang Y, Zhang Z, Huang J, Li C, (2020) Li_{6.7}La₃Zr_{1.7}Ta_{0.15}Nb_{0.15}O₁₂ enhanced UV-cured poly(ethylene oxide)-based composite gel polymer electrolytes for lithium metal batteries. *Electrochim Acta* 360:137014 <https://doi.org/10.1016/j.electacta.2020.137014>
47. Wang C, Gong Y, Liu B, Fu K, Yao Y, Hitz E, Li Y, Dai J, Xu S, Luo W, Wachsmann ED, Hu L (2017) Conformal, nanoscale ZnO surface modification of garnet-based solid-state electrolyte for lithium metal anodes. *Nano Lett* 17(1):565–571. <https://doi.org/10.1021/acs.nanolett.6b04695>
48. Xie Z, Wu Z, An X, Yoshida A, Wang Z, Hao X, Abudula A, Guan G (2019) Bifunctional ionic liquid and conducting ceramic co-assisted solid polymer electrolyte membrane for quasi-solid-state lithium metal batteries. *J Membr Sci* 586:122–129. <https://doi.org/10.1016/j.memsci.2019.05.066>
49. Yang X, Jiang M, Gao X, Bao D, Sun Q, Holmes N, Duan H, Mukherjee S, Adair K, Zhao C, Liang J, Li W, Li J, Liu Y, Huang H, Zhang L, Lu S, Lu Q, Li R, Singh CV, Sun X (2020) Determining the limiting factor of the electrochemical stability window for PEO-based solid polymer electrolytes: main chain or terminal -OH group? *Energy Environ Sci* 13:1318–1325. <https://doi.org/10.1039/d0ee00342e>

Publisher's note Springer Nature remains neutral with regard to jurisdictional claims in published maps and institutional affiliations.